Ab Initio and Molecular Dynamics Studies of Crystalline TNAD (*trans*-1,4,5,8-Tetranitro-1,4,5,8-tetraazadecalin)

Ling Qiu, He-Ming Xiao,* Wei-Hua Zhu, Ji-Jun Xiao, and Wei Zhu

Department of Chemistry, Nanjing University of Science and Technology, Nanjing 210094, People's Republic of China

Received: March 19, 2006; In Final Form: April 11, 2006

The structural and electronic properties of the energetic crystal TNAD (*trans*-1,4,5,8-tetranitro-1,4,5,8-tetraazadecalin) have been studied using plane-wave ab initio calculations based on the density function theory method with the ultrasoft pseudopotentials. It is found that the predicted crystal structure is in good agreement with experimental data and there are strong inter- and intramolecular interactions in bulk TNAD. Band structure calculations indicate that TNAD is an insulator with the band gap of ca. 3.3 eV. The hydrostatic compression effect on TNAD has been studied in the pressure range of 0−600 GPa. The results show that a pressure less than 10 GPa does not significantly change the geometric parameters, charge distributions, and electronic bands. When the pressure is over 10 GPa, increasing the pressure determines significant changes of the geometrical and electronic structures and large broadening of the electronic bands together with a sharp decrease of the band gap. Isothermal−isobaric molecular dynamics simulations at atmospheric pressure were further performed on the TNAD crystal in the temperature range 5−500 K. Average equilibrium lattice parameters and elastic properties as functions of temperature were determined. The thermal expansion coefficients calculated for the crystal indicate anisotropic behavior with the largest expansion along the *b* axis.

1. Introduction

As is well known, nitramines have had important applications in both the civilian and military fields for a long time. This group of compounds is still a source of explosives and propellants that possess predominantly high energy contents.[1−3] At present, the attractive nitramines involve a series of polycyclic polynitramines, which have an optimum number of nitro groups, improved crystal density, and higher stored energies. On the other hand, the ongoing research work on the syntheses of such compounds is based on the fact that they generally have higher densities and oxygen balance than their corresponding open counterparts and carbocyclic analogues, which is important for increasing the performance of energetic materials.[4] Among them, the explosive *trans*-1,4,5,8-tetranitro-1,4,5,8-tetraazadecalin (TNAD)[5] (see Figure 1 for the structural diagram of the molecule) has attracted much attention[6−13] since it was synthesized. It was characterized as a promising high energy density material (HEDM) with low shock sensitivity and good thermal stability. Its melting point is reported at 232−234 °C,[5] and it decomposes only above 220 °C according to thermogravimetry (TG) and differential thermal analysis (DTA).[9] Its measured impact sensitivity (in terms of the height from which a falling 2.5 kg weight will cause detonation 50% of the time) is 35 cm, comparable to the values of 25−28 cm for RDX (1,3,5-trinitro-1,3,5-triazocyclohexane) and 18−26 cm for HMX (1,3,5,7-tetranitro-1,3,5,7-tetraazacyclo octane) that are among the most effective and widely used explosives and monopropellants.[5,7a] So, a further interesting point about TNAD is what causes the lower sensitivity relative to RDX and HMX.

So far, there have been several theoretical studies on TNAD. The relationships between shock sensitivity, bond strength, and molecular size have been studied using an ab initio self-consistent filed molecular orbital approach at the 3-21G level by Politzer et al.[8] Sorescu et al. have developed a "transferable" intermolecular potential and have applied it within a rigid-molecule framework to a number of high explosives, including TNAD.[11] Liu et al. have predicted the detonation properties of TNAD and its hypothesized molecular derivatives by using a hybrid B3LYP density functional theory (DFT) method.[12] Recently, the thermodynamic properties and detonation performance of TNAD and its isomers have been calculated at the B3LYP/6-31G* level by our workgroup.[13]

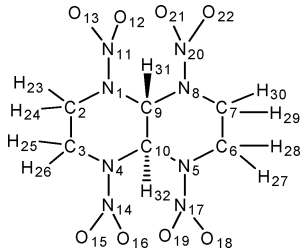

Figure 1. Schematic view of the structure and atomic numbering of the TNAD molecule.

It is known that intra- and intermolecular forces control diverse phenomena such as diffusion, aggregation, and detonation. It is also acknowledged that the performance of an explosive basically depends on the solid condition such as its crystal structure, since the intra- and intermolecular interactions influence the strengths of some weak bonds that are referred to as initiators in the decomposition or detonation processes. Therefore, to provide the fundamental information, it is necessary to study the molecule in the crystalline phase. However, to the best of our knowledge, there is no such investigation on TNAD until now. In the present work, we extend our previous theoretical investigations by considering the effects of the

* To whom correspondence should be addressed. Tel. and fax: +86-25-84303919. E-mail: xiao@mail.njust.edu.cn.

10.1021/jp061707w CCC: $33.50
Published on Web 05/12/2006

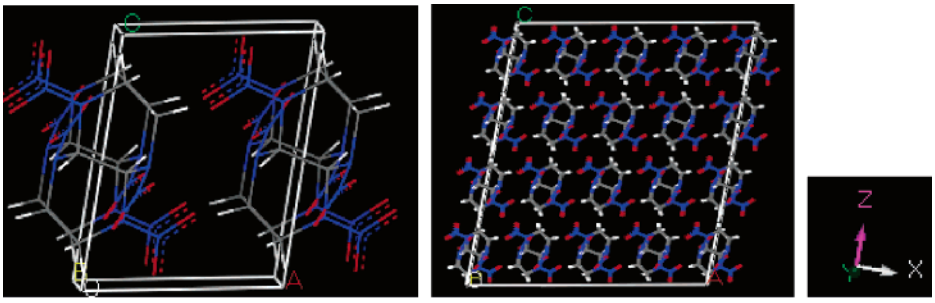

(a) (b)

Figure 2. Perspective view of bulk TNAD (a) and the periodic MD simulation cell (a 4 × 4 × 4 box of unit cells) along the *b* axis (b).

crystalline field on the geometric and electronic parameters of TNAD to explore the fundamental behavior of this system and to better understand the basic characteristics of energetic materials that determine shock sensitivity. First-principles calculations based on DFT with ultrasoft pseudopotentials were performed to determine the structural and electronic properties of the TNAD crystal. Furthermore, understanding the combustion and detonation processes of energetic materials is another important task since their mechanisms are not well-known. It was suggested that initiation of these processes in solid energetic materials is associated with the presence of "hot spots"[14] or regions of high shear stress[15] determined by a high density of dislocations. However, Gilman questioned this interpretation and emphasized the role of the excited electronic states in initiating these processes.[16] In particular, he suggested that shock initiation can be determined by metallization of the solid as a result of highly compressed materials. Given the importance of the role caused by compression effects on the electronic structures of solids, we analyzed such effects on TNAD in the present study based on the plane-wave ab initio calculations in the pressure range of 0−600 GPa. This procedure has been used widely and shown to be meaningful in better understanding the crystallographic phase transitions and thermolysis or detonation mechanisms of the solid energetic materials.[17−20]

Moreover, recently, plenty of attention has been paid to the structural, thermodynamic, and mechanical properties of explosives and plastic-bonded explosives (PBXs) by using molecular dynamics simulations.[18,21−25] Ideally, a more realistic prediction of the equilibrium and dynamical properties for the molecular crystals would be obtained from first-principles molecular dynamics simulations. Such calculations are state-of-the-art but extremely computationally demanding. An alternative to this approach is to use classical molecular dynamics (MD) or Monte Carlo (MC) simulations with an empirical force field. As far as we know, there is no report on the structure and performances of the crystalline TNAD using these methods. So, isothermal−isobaric molecular dynamics simulations (NPT-MD) with the COMPASS force field[26] as a function of temperature over the range of 5−500 K at ambient pressure were performed on the TNAD crystal.

The organization of this paper is as follows: In section 2, we describe the computational methodology. The results of ab initio total energy calculations and isothermal−isobaric molecular dynamics simulations are presented in section 3. The main conclusions are summarized in section 4.

2. Computational Method

2.1. Density Functional Theory Calculations. The ab initio calculations performed in this study were done within the framework of DFT[27] using Vanderbilt-type ultrasoft pseudopotentials[28] and a plane-wave expansion of the wave functions. These pseudopotentials permit the use of lower plane-wave cutoff energies than would be required with standard norm-conserving pseudopotentials. The self-consistent ground state of the system was determined using a band-by-band conjugate gradient technique to minimize the total energy of the system with respect to the plane-wave coefficients. The electronic wave functions were obtained by the Pulay density-mixing scheme,[29] and the structures were relaxed using the Broyden−Fletcher−Goldfarb−Shanno (BFGS) method.[30] The local density approximation (LDA) with the Ceperley−Alder[31] exchange-correlation potential as parametrized by Perdew and Zunger[32] was employed. The cutoff energy of plane waves was set to 400.0 eV. Brillouin zone sampling was performed using the special Monkhost−Pack scheme[33] with a *k*-point grid of 3 × 3 × 3. This is sufficiently accurate for the molecular crystal TNAD since we find that its energy bands are fairly flat.

The initial TNAD crystal structure taken from Willer and Lowe-Ma[7b] was used for the computations of the bulk. It crystallizes in space group *P*-1 with six independent lattice parameters $a = 6.461$ Å, $b = 6.845$ Å, $c = 7.542$ Å, $\alpha = 74.01°$, $\beta = 75.00°$, and $\gamma = 68.53°$. And, there is one irreducible molecule in the unit cell (see Figure 2a). Periodic nature of the crystal has been considered by using periodic boundary conditions in all three directions. The full relaxation of the structure was performed to allow the atomic configurations, cell shape, and volume to change. In the geometry relaxation, the total energy of the system was converged less than 2.0×10^{-5} eV, the residual force less than 0.05 eV/Å, the displacement of atoms less than 0.002 Å, and the residual bulk stress less than 0.1 GPa. Besides optimization of the crystal at ambient pressure, we have done calculations at different pressures in the range of 0−600 GPa.

2.2. Molecular Dynamics Simulations. A more comprehensive understanding of the intra- and intermolecular interactions in the TNAD crystal has been achieved by constant pressure and temperature (NPT) molecular dynamics simulations using the commercial software Accelrys Materials Studio (MS) 3.0.1[34] with the Discover package. This method yields average equilibrium properties of the lattice as functions of temperature and pressure. The Andersen temperature control method[35] and the Parrinello barostat method[36] were used to simulate the crystal at atmospheric pressure in the temperature range 5−500 K.

The periodic MD simulation cell containing 64 molecules shown in Figure 2b is used for TNAD, corresponding to a 4 × 4 × 4 box of unit cells. In the initial simulation corresponding to the lowest temperature, the position and orientation of the molecules in the bulk were taken to be identical to those of the experimental structure. The system was integrated for 1×10^5 time steps in all the equilibration runs, followed by the

TABLE 1: Comparison of Relaxed Lattice Parameters, Unit Cell Volume, and Density for TNAD with Experimental Results[a]

	lattice parameters							
method	*a* (Å)	*b* (Å)	*c* (Å)	α (deg)	*β* (deg)	*γ* (deg)	*V* (Å^3)	*ρ* (g/cm^3)
LDA/CA-PZ	6.417(−0.68)	6.829(−0.23)	7.555(0.17)	74.931(1.24)	75.369(0.49)	69.523(1.45)	294.664(0.33)	1.816(−0.33)
GGA/PBE	6.590(2.00)	7.028(2.67)	7.717(2.32)	74.100(0.12)	75.195(0.26)	69.838(1.91)	317.527(8.11)	1.685(−7.52)
exp (ref 7b)	6.461	6.845	7.542	74.010	75.000	68.530	293.704	1.822

[a] The values in parentheses correspond to the percentage differences relative to the experimental data.

TABLE 2: Variations of the Lattice Parameters, Unit Cell Volume, and Density of TNAD as Functions of the Applied Hydrostatic Pressure[a]

	lattice parameters							
P (GPa)	*a* (Å)	*b* (Å)	*c* (Å)	α (deg)	*β* (deg)	*γ* (deg)	*V* (Å^3)	*ρ* (g/cm^3)
0	6.394	6.829	7.559	75.003	75.437	70.042	294.771	1.815
	(−1.04)	(−0.23)	(0.23)	(1.34)	(0.58)	(2.21)	(0.36)	(−0.38)
0.0001	6.417	6.829	7.555	74.931	75.369	69.523	294.664	1.816
	(−0.68)	(−0.23)	(0.17)	(1.24)	(0.49)	(1.45)	(0.33)	(−0.33)
0.1	6.414	6.827	7.550	74.938	75.370	69.526	294.252	1.818
	(−0.73)	(−0.26)	(0.11)	(1.25)	(0.49)	(1.45)	(0.19)	(−0.22)
1	6.386	6.795	7.512	74.838	75.379	69.495	289.980	1.845
	(−1.16)	(−0.73)	(−0.40)	(1.12)	(0.51)	(1.41)	(−1.27)	(1.26)
10	6.111	6.518	7.202	74.311	75.019	69.056	253.725	2.109
	(−5.42)	(−4.78)	(−4.51)	(0.41)	(0.03)	(0.77)	(−13.61)	(15.75)
100	5.146	5.580	6.135	78.014	71.976	66.280	152.654	3.505
	(−20.35)	(−18.48)	(−18.66)	(5.41)	(−4.03)	(−3.28)	(−48.02)	(92.37)
200	4.630	5.257	5.771	80.990	74.123	69.522	126.281	4.237
	(−28.34)	(−23.20)	(−23.48)	(9.43)	(−1.17)	(1.45)	(−57.00)	(132.55)
400	4.023	4.735	5.377	84.451	81.760	83.196	100.320	5.333
	(−37.73)	(−30.83)	(−28.71)	(14.11)	(9.01)	(21.40)	(−65.84)	(192.70)
600	3.982	4.922	4.732	83.902	80.799	76.093	88.641	6.036
	(−38.37)	(−28.09)	(−37.26)	(13.37)	(7.73)	(11.04)	(−69.82)	(231.28)
exp (ref 7b)	6.461	6.845	7.542	74.010	75.000	68.530	293.704	1.822

[a] The values in parentheses correspond to the percentage differences relative to the experimental data.

production runs of 2×10^5 time steps, during which data were collected for subsequent analysis. A fixed time step size of 1 fs was used in all cases. The mechanical properties were estimated by the static mechanics method as implemented in the MS 3.0.1 program, and the values were obtained by averaging the mechanical properties of five configurations. In these calculations, the interactions were determined between the sites in the simulation box and the nearest-image sites within the cutoff distance 9.5 Å. The Coulombic and van der Waals long-range interactions were handled by using the standard Ewald's method.[37] The periodic boundary condition was also employed in all simulations. All calculations were performed on a Pentium-IV personal computer.

3. Results and Discussion

3.1. DFT Calculations. *3.1.1. Crystal Structure*. Before carrying out the calculations reported here, we applied two different functionals, LDA and GGA (generalized gradient approximation), to the bulk TNAD as a test. The calculated lattice parameters, unit cell volume, and crystalline density of bulk TNAD are given in Table 1 together with the experimental data.[7b] It is found that the LDA well reproduces the lattice constants of bulk TNAD, whereas the GGA slightly increases them, in comparison with the experiment. The LDA results give the lattice constants $a = 6.417$ Å, $b = 6.829$ Å, $c = 7.555$ Å, $\alpha = 74.931°$, $\beta = 75.369°$, and $\gamma = 69.523°$, in good agreement with the experimental values.[7b] The relative errors for *a*, *b*, *c*, α, *β*, and *γ* are −0.68%, −0.23%, 0.17%, 1.24%, 0.49%, and 1.45%, respectively. The unit cell volume calculated by this function agrees well with the experimental data, with a difference of only 0.33%. However, the GGA overestimates the cell volume of TNAD by 8.11% and, therefore, results in a lower crystalline density with an error of −7.52%, which is typical for the GGA method. These comparisons appear to show that the LDA results are reasonably satisfactory. Consequently, in further calculations, we shall use the LDA (CA-PZ), which may be expected to produce more reliable predictions of the structures. The changes of the TNAD band gap and density of states under hydrostatic compression are also obtained from the LDA calculations. Even though the LDA gap itself is well-known to be underestimated, the LDA pressure derivative of gap has been shown to be reliable.[38]

To check the effect of hydrostatic compression on the crystal structure, we compared the calculated crystallographic lattice parameters, volume, and density for the TNAD unit cell in the pressure range of 0−600 GPa with the experimental data in Table 2. The compressibility of TNAD was investigated. The results show that, in the lower pressure regime (below 10 GPa), the lattice parameters, cell volume, and crystalline density change slightly and agree reasonably with the experimental data. In the region of higher pressures (above 10 GPa), these parameters change largely and the errors relative to the experimental values increase. The lattice dimensions are compressed greatly, and the crystalline density of TNAD increases significantly with the increasing pressure. When the pressure arrives at 600 GPa, the density increases 231.28% in comparison with the experimental data. Because the detonation velocity and pressure increase tremendously with the increasing density and its square, respectively,[4] it is crucial to increase the density for improving the performance of an explosive or propellant. On the other hand, conventionally, a compound can be considered as a high energy density compound (HEDC) if its density is larger than 1.9 g/cm^3, detonation velocity is greater than 9 km/s, and detonation pressure is over 40 GPa. Consequently, we infer that one can increase the solid-state density of TNAD over 2.1 g/cm^3 by compressing it under tens of gigapascals of

TABLE 3: Variations of Intra- and Intermolecular Geometrical Parameters in TNAD as Functions of Pressure

		P (GPa)								
bond	exp (ref 7b)	0	0.0001	0.1	1	10	100	200	400	600
C2−C3	1.544	1.531	1.531	1.531	1.530	1.525	1.436	1.382	1.322	1.250
C9−C10	1.531	1.529	1.529	1.529	1.529	1.526	1.462	1.404	1.309	1.271
N1−C2	1.462	1.439	1.439	1.439	1.438	1.434	1.367	1.339	1.266	1.253
N1−C9	1.457	1.424	1.424	1.424	1.423	1.422	1.378	1.339	1.271	1.251
N4−C3	1.497	1.455	1.454	1.454	1.454	1.452	1.388	1.335	1.287	1.231
N4−C10	1.468	1.452	1.452	1.452	1.451	1.445	1.371	1.328	1.288	1.248
N1−N11	1.370	1.369	1.369	1.369	1.368	1.358	1.303	1.302	1.294	1.294
N4−N14	1.377	1.363	1.363	1.363	1.362	1.356	1.312	1.268	1.293	1.259
N11−O12	1.229	1.248	1.248	1.248	1.248	1.250	1.230	1.211	1.253	1.209
N11−O13	1.223	1.242	1.242	1.242	1.243	1.244	1.224	1.213	1.219	1.184
N14−O15	1.228	1.248	1.247	1.247	1.248	1.247	1.215	1.188	1.196	1.202
N14−O16	1.231	1.250	1.250	1.250	1.250	1.250	1.224	1.208	1.225	1.212
C2−H23	0.967	1.101	1.101	1.101	1.101	1.098	1.067	1.055	1.017	2.635
C2−H24	0.961	1.105	1.105	1.105	1.105	1.104	1.071	1.042	0.998	0.989
C3−H25	0.960	1.104	1.104	1.104	1.104	1.103	1.079	1.063	1.013	0.999
C3−H26	0.961	1.106	1.106	1.106	1.106	1.103	1.064	1.046	1.043	1.036
C9−H31	0.964	1.113	1.113	1.113	1.114	1.112	1.087	1.073	1.056	1.021
O12···H31	2.274	2.297	2.297	2.299	2.307	2.312	2.276	2.176	2.023	1.365
O13···H23	2.253	2.216	2.216	2.217	2.218	2.229	1.905	1.612	1.439	1.383
O15···H26	2.296	2.218	2.218	2.219	2.219	2.200	1.895	1.794	1.658	1.454
O16···H31	2.729	2.660	2.647	2.647	2.646	2.613	2.558	2.481	2.444	2.346
O12···H24[a]	2.699	2.510	2.510	2.506	2.482	2.286	1.850	1.809	1.709	1.027
O12···H32[a]	2.506	2.306	2.306	2.304	2.282	2.079	1.536	1.442	1.341	1.311
O15···H30[a]	2.474	2.334	2.331	2.328	2.317	2.180	1.996	1.911	1.862	1.692
O16···H23[a]	2.630	2.550	2.550	2.545	2.508	2.252	1.921	1.808	1.677	1.594
O16···H27[a]	2.507	2.353	2.345	2.344	2.344	2.321	2.309	2.213	1.882	1.115
O16···H29[a]	2.699	2.558	2.558	2.557	2.534	2.357	1.994	1.699	1.671	1.579

[a] Hydrogen atom of another molecule.

pressure to improve its detonation velocity and pressure. This will be instructive and useful for the molecular design of novel HEDMs.

It is also noteworthy that the compressibility of TNAD is anisotropic at low or high pressure. The structure is much stiffer in the *b* and *c* directions than along the *a* direction. This different behavior can be understood based on the type of bonding for this crystal. There exist strong electrostatic interactions in the *bc* plane and somewhat weaker interactions along the *a* direction. Consequently, it is expected that the compressibility properties of TNAD will be similar for the *b* and *c* directions but different from the *a* direction, which has the highest compressibility. Further, there are some breaks in the lattice parameters *b*, α, β, and γ of the crystal TNAD at 400 GPa. This means that a phase transition may take place in TNAD at about this pressure and other crystallographic packings may be possible for TNAD in the higher pressure region.

3.1.2. Geometrical Structure. The calculated intra- and intermolecular geometrical parameters of TNAD are given in Table 3. Since TNAD is centrosymmetric in the both theoretical and experimental structures, only half of the geometrical parameters are presented. Analysis of the results in Table 3 shows that the optimized bond distances at ambient pressure agree reasonably with the experimental values. The largest deviations appear for the C−H bonds as well as for the O···H hydrogen bonds. For the C−H bonds, our calculation gives the values around 1.101−1.113 Å, whereas the experimental values vary from 0.960 to 0.967 Å. Similarly, the predicted O···H intramolecular distances range between 2.216 and 2.647 Å, which are smaller than the experimental values that vary from 2.253 to 2.729 Å. The calculated O···H intermolecular distances range between 2.306 and 2.558 Å, also shorter than the experimental values that vary from 2.474 to 2.699 Å. The main reason for such differences is the uncertainty in the H-atom positions obtained using X-ray diffraction, which determines the centers of charge for H atoms and not the positions of the nuclei. Additionally, our observation is in agreement with the experiment that the shortest hydrogen bonds are intramolecular, whereas the other bonds are intermolecular, indicated in Table 3. This extensive intra- and intermolecular hydrogen bonding network is found to be responsible for the limited amount of thermal motion of the individual atoms as well as for the low sensitivity to friction and impact of the TNAD crystal.[5,7a]

Furthermore, the influences of pressure on the bond distances have been studied in the range of 0−600 GPa. As can be seen from Table 3, in the low pressure range (below 10 GPa), the bond distances in TNAD decrease slightly with the pressure increases, while all the intermolecular hydrogen bonds decrease markedly although some intramolecular hydrogen bonds increase a little such as O12···H31, O13···H23, and O15···H26. When in the region of higher pressures, with the pressure increasing from 10 to 600 GPa, most of the atomic distances in the TNAD crystal decrease largely as expected especially under the pressure of 600 GPa. At present, the crystal structure has been changed greatly. Some of the intra- and intermolecular O···H nonbonded contacts have become so close that practically new covalent O−H bonds are formed. For example, the shortest intramolecular hydrogen bonds O12···H31, O13···H23, and O15···H26 are 1.365, 1.383, and 1.454 Å, respectively; the shortest intermolecular hydrogen bonds O12···H24, O12···H32, and O16···H27 are 1.027, 1.311, and 1.115 Å, respectively. Moreover, the electron-withdrawing effect of the nitro groups leads to the phenomenon that the oxygen atoms involved in strong hydrogen bonds (such as O12 and O16) form longer N−O bonds. Similarly, longer C−H bonds are formed since the hydrogen atoms (H23, H26, and H31) are involved in strong intra- and intermolecular hydrogen bonds. However, it should be also noticed that there is some abnormal behavior for the geometrical parameters of TNAD at 400 GPa, which is consistent with the changes of the lattice parameters. This further

TABLE 4: Variations of the Mulliken Atomic Charges in TNAD as Functions of Pressure

	P (GPa)								
atom	0	0.0001	0.1	1	10	100	200	400	600
C2	−0.44	−0.44	−0.44	−0.44	−0.41	−0.26	−0.23	−0.23	0.09
C3	−0.44	−0.44	−0.44	−0.43	−0.41	−0.30	−0.28	0.08	−0.20
C9	−0.03	−0.03	−0.03	−0.02	−0.02	0.01	0.03	0.05	−0.02
N1	−0.14	−0.14	−0.14	−0.14	−0.13	−0.10	−0.09	−0.13	−0.11
N4	−0.15	−0.15	−0.15	−0.15	−0.14	−0.13	−0.11	−0.08	−0.12
N11	0.53	0.53	0.53	0.53	0.52	0.49	0.47	0.45	0.44
N14	0.51	0.51	0.51	0.51	0.50	0.48	0.45	0.29	0.27
O12	−0.40	−0.40	−0.40	−0.40	−0.40	−0.38	−0.38	−0.39	−0.39
O13	−0.39	−0.39	−0.39	−0.39	−0.39	−0.39	−0.39	−0.47	−0.49
O15	−0.42	−0.42	−0.42	−0.42	−0.43	−0.45	−0.45	−0.56	−0.58
O16	−0.40	−0.40	−0.40	−0.40	−0.39	−0.34	−0.34	−0.29	−0.20
H23	0.36	0.36	0.36	0.36	0.34	0.26	0.24	0.26	0.24
H24	0.34	0.34	0.34	0.34	0.33	0.25	0.24	0.24	0.30
H25	0.35	0.35	0.34	0.34	0.33	0.27	0.26	0.23	0.29
H26	0.35	0.35	0.35	0.35	0.33	0.27	0.27	0.27	0.17
H31	0.37	0.37	0.37	0.37	0.36	0.32	0.31	0.28	0.31

suggests that a phase transition may take place in the crystal at about 400 GPa.

3.1.3. Atomic Charges and Bond Overlap Populations. Table 4 lists the atomic charge distributions in TNAD and the individual atomic charge variations resulting from the anisotropic hydrostatic compressions, which can describe the effect of charge rearrangement caused by the compression of the lattice intuitively. Only half of the atomic charges are presented due to the fact that TNAD is centrosymmetric. As can be seen in Table 4, the hydrogen and nitro-N atoms carry a lot of positive charges, while the carbon, oxygen, and nitrogen atoms on the ring contact with the nitro group bear lots of negative charges. However, it is noted that the carbon atoms on the bridge, i.e., C9 and C10, carry nearly zero charges. This is because the negative charges of the nitrogen atoms connected to the bridge carbon atoms neutralize the positive charges of the hydrogen atoms to the same ones on the whole.

Let us examine the detailed modifications of charge distribution resulting from the anisotropic compressions. For a decrease of about 5% of the cell axes *a*, *b*, and *c* with the pressure increasing from 0 to 10 GPa, all the atomic charges in the bulk scarcely change. While the pressure increases from 10 to 600 GPa, the variations of charges on the nitrogen atoms in the ring skeleton (i.e., N1, N4, N5, and N8) and in the nitro groups (i.e., N11, N14, N17, and N20) inversely evolve with the increasing pressure, namely, they increase for the nitrogen atoms in the ring skeleton and decrease for those of the nitro groups. These changes take place together with a decrease in the charges of H atoms and a significant increase in the charges on the O atoms of the nitro groups involved in more hydrogen bondings, such as the O12 and O16 atoms. The charges on all the carbon atoms also increase as the pressure increases. The clear and large charge transfer and redistribution among the atoms can be seen as a result of the lattice compressions.

An alternative way to describe the charge rearrangement caused by the compression of the lattice has been obtained by evaluating the Mulliken bonding overlap populations of different bonds in the system. However, it is known that Mulliken population analysis[39] suffers from some shortcomings, especially the basis set dependence. But, for the purpose of comparing trends in the electron distribution for homologous compounds at the same calculation condition, results derived from Mulliken population analysis are still meaningful. As our goal here is to draw the variation trend of electron distribution in the same system with the external pressure changing, a conclusion based on Mulliken population analysis would be reasonable. Table 5

TABLE 5: Variations of Mulliken Bonding Populations for TNAD as Functions of Pressure

	P (GPa)								
bond	0	0.0001	0.1	1	10	100	200	400	600
C2−C3	0.67	0.67	0.67	0.67	0.68	0.75	0.81	0.88	1.05
C9−C10	0.72	0.72	0.72	0.72	0.72	0.75	0.78	0.87	1.07
N1−C2	0.66	0.66	0.66	0.66	0.67	0.73	0.79	0.88	0.92
N1−C9	0.77	0.77	0.77	0.77	0.77	0.79	0.84	0.92	0.98
N4−C3	0.65	0.65	0.65	0.65	0.65	0.73	0.81	0.89	1.03
N4−C10	0.66	0.66	0.66	0.66	0.66	0.71	0.75	0.83	0.86
N1−N11	0.71	0.71	0.71	0.71	0.73	0.81	0.79	0.76	0.56
N4−N14	0.73	0.73	0.73	0.73	0.74	0.78	0.82	0.62	0.84
N11−O12	0.75	0.75	0.75	0.75	0.75	0.76	0.81	0.67	0.68
N11−O13	0.76	0.76	0.76	0.76	0.76	0.81	0.86	0.75	0.76
N14−O15	0.74	0.74	0.74	0.74	0.75	0.78	0.76	0.63	0.72
N14−O16	0.74	0.74	0.74	0.74	0.74	0.82	0.85	0.74	0.68
C2−H23	0.82	0.82	0.82	0.82	0.85	1.06	1.14	1.17	1.31
C2−H24	0.84	0.84	0.84	0.84	0.85	1.05	1.19	1.32	−0.03
C3−H25	0.81	0.81	0.81	0.81	0.83	1.00	1.03	1.16	0.94
C3−H26	0.82	0.82	0.82	0.82	0.85	1.02	1.08	1.18	1.29
C9−H31	0.87	0.87	0.87	0.87	0.88	0.92	0.96	0.97	1.00
O12···H31	0.00	0.00	0.00	0.00	0.00	0.00	−0.01	−0.04	0.15
O13···H23	0.01	0.01	0.01	0.01	0.01	0.01	0.04	0.09	0.15
O15···H26	0.01	0.01	0.01	0.01	0.01	−0.01	−0.02	−0.05	0.06
O16···H31	0.00	0.00	0.00	0.00	0.00	0.02	0.02	0.00	0.02
O12···H24[a]	0.01	0.01	0.01	0.01	0.01	0.01	−0.05	−0.15	0.67
O12···H32[a]	0.00	0.00	0.00	0.00	0.01	0.08	0.11	0.16	−0.04
O15···H30[a]	0.00	0.00	0.00	0.00	0.00	−0.06	−0.11	−0.13	−0.22
O16···H23[a]	0.00	0.00	0.00	0.00	−0.01	−0.08	−0.13	−0.17	−0.39
O16···H27[a]	0.00	0.00	0.00	0.00	0.00	−0.01	0.01	0.06	0.42
O16···H29[a]	0.00	0.00	0.00	0.00	0.01	−0.01	−0.04	−0.15	−0.15

[a] Hydrogen atom of another molecule.

collects the bond overlap populations of the TNAD crystal obtained from the Mulliken population analysis as well as the variations of those caused by the anisotropic hydrostatic compressions. Inspecting the data in Table 5, it can be found that, in the lower pressure ranges (below 10 GPa), overlap populations of the $N-NO_2$, C−C, and C−N bonds are close to each other, which means that thermolysis or detonation of TNAD could be initiated by the $N-NO_2$ bond homolysis as well as breaking the ring at the C−C and C−N bonds. The intra- and intermolecular interactions are very weak according to the calculated bonding populations. Additionally, these overlap populations hardly change as the pressure increases from 0 to 10 GPa. In the higher pressure region (above 200 GPa), most bonding overlap populations increase with the increasing pressure, while some bonds have smaller values compared with those in the lower pressure region, such as the N1−N11, N11−O12, and N14−O16 bonds. These are the result of electron transfer caused by the anisotropic compression of the bulk. Especially, the N1−N11 bond has the smallest population among these bonds and the populations of intra- and intermolecular hydrogen bonds have increased largely under the external pressure of 600 GPa. In general, bonds with smaller populations are relatively weaker and less resistant to rupture. Therefore, we infer that the $N-NO_2$ bond of TNAD is the weakest under higher pressure, that is, TNAD could be pyrolyzed by initially rupturing the $N-NO_2$ bond rather than the other bonds in the decomposition or detonation processes under higher pressure. At the same time, hydrogen transfer is also a minor pathway for the decomposition of TNAD, which is consistent with the previous investigations on the thermolysis of nitramines.[40] In other words, an anisotropic impact on the bulk may initiate the rupture of the $N-NO_2$ bond and the transfer of the hydrogen atoms. These also demonstrate that there are strong intra- and intermolecular interactions in the bulk under higher pressures, while electron flow leads to the destabilization of the crystalline TNAD. In the overall pressure range, another striking feature

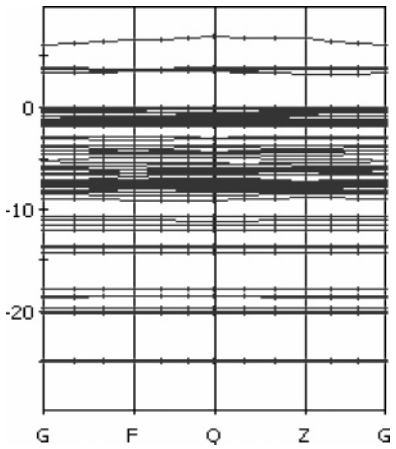

Figure 3. Calculated band structure of TNAD along different symmetry directions of the Brillouin zone.

for the TNAD Mulliken populations is that the bond overlap populations change abnormally from 400 to 600 GPa, which agrees well with the variations of the charge distributions and geometrical parameters. This further implies that the crystal structure of TNAD has been changed under high pressure.

3.1.4. Band Structure and Density of States. The self-consistent band structure along different symmetry directions of the Brillouin zone for the optimized structure of bulk TNAD has been calculated by the LDA. The result is shown in Figure 3, and the corresponding total density of states (DOS) is given in Figure 4. In Figures 3 and 4, the energy of the highest occupied crystalline orbital (HOCO) has been set to zero. As can be seen from Figure 3, TNAD is an electrical insulator with a band gap of 3.27 eV at the Z point. The bands are almost flat along the Brillouin zone, consistent with the character of the molecular crystal. The real band gap may be slightly larger since LDA calculations generally underestimate the band gap. Therefore, we have also performed GGA calculations in order to test whether GGA would improve the performance of the LDA on the energy band gap. Note that there is only a little discrepancy between the band gaps of the GGA and LDA. The GGA/PBE (Perdew−Burke−Ernzerhof) calculation shows a slightly larger value of 3.39 eV for the band gap of TNAD.

A better understanding the character of these bands can be obtained by projecting the calculated electronic density on the atom-centered orbitals. These representations, called the projected density of states (PDOS), are given in Figure 4 for the case of individual atoms C2, C3, C9, N1, N4, N11, N14, O12, O13, O15, O16, H23, H24, H25, H26, and H27 in the TNAD molecule. We only presented the PDOS on half of the atoms as TNAD has C_i symmetry, and the other PDOSs are similar. As shown in Figure 4, the individual s and p bands correspond-

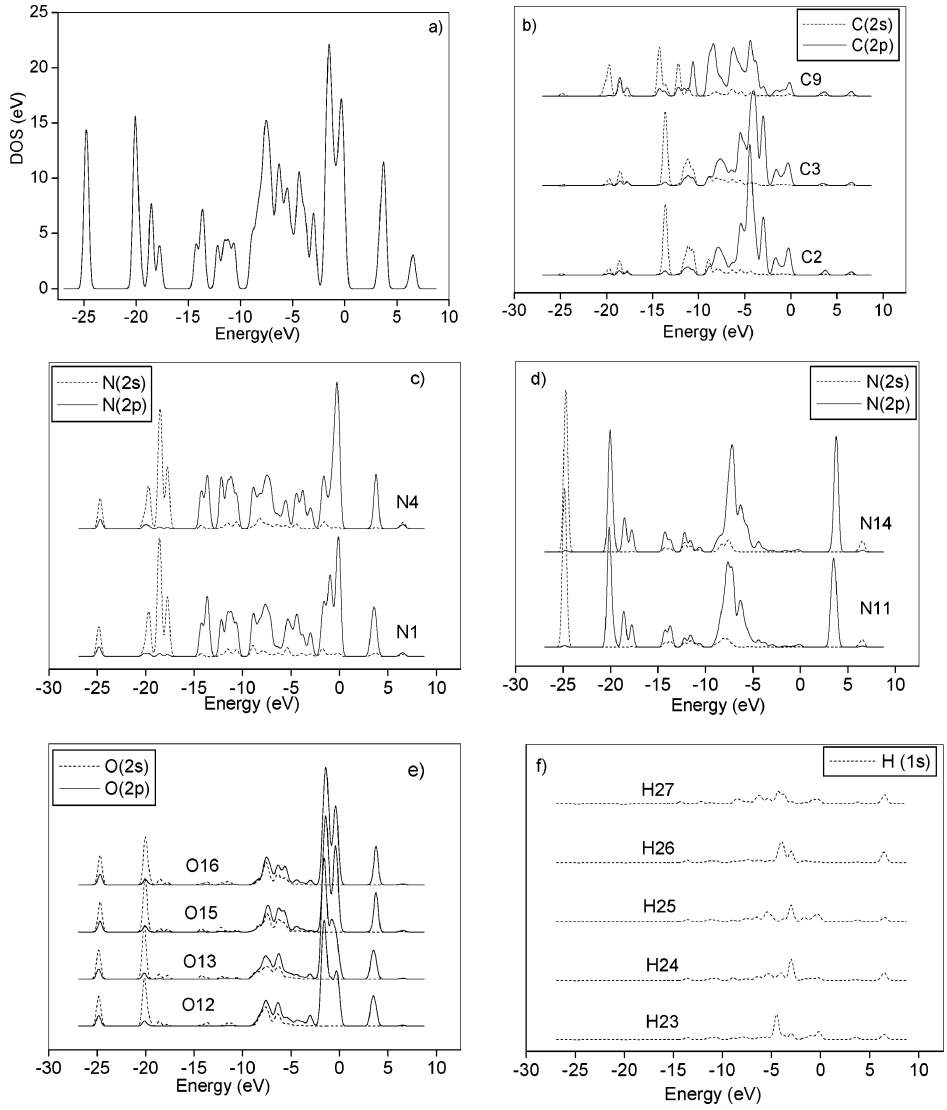

Figure 4. Calculated total density of states (DOS) of TNAD (a) and the projected density of states (PDOS) on individual atoms (b−f).

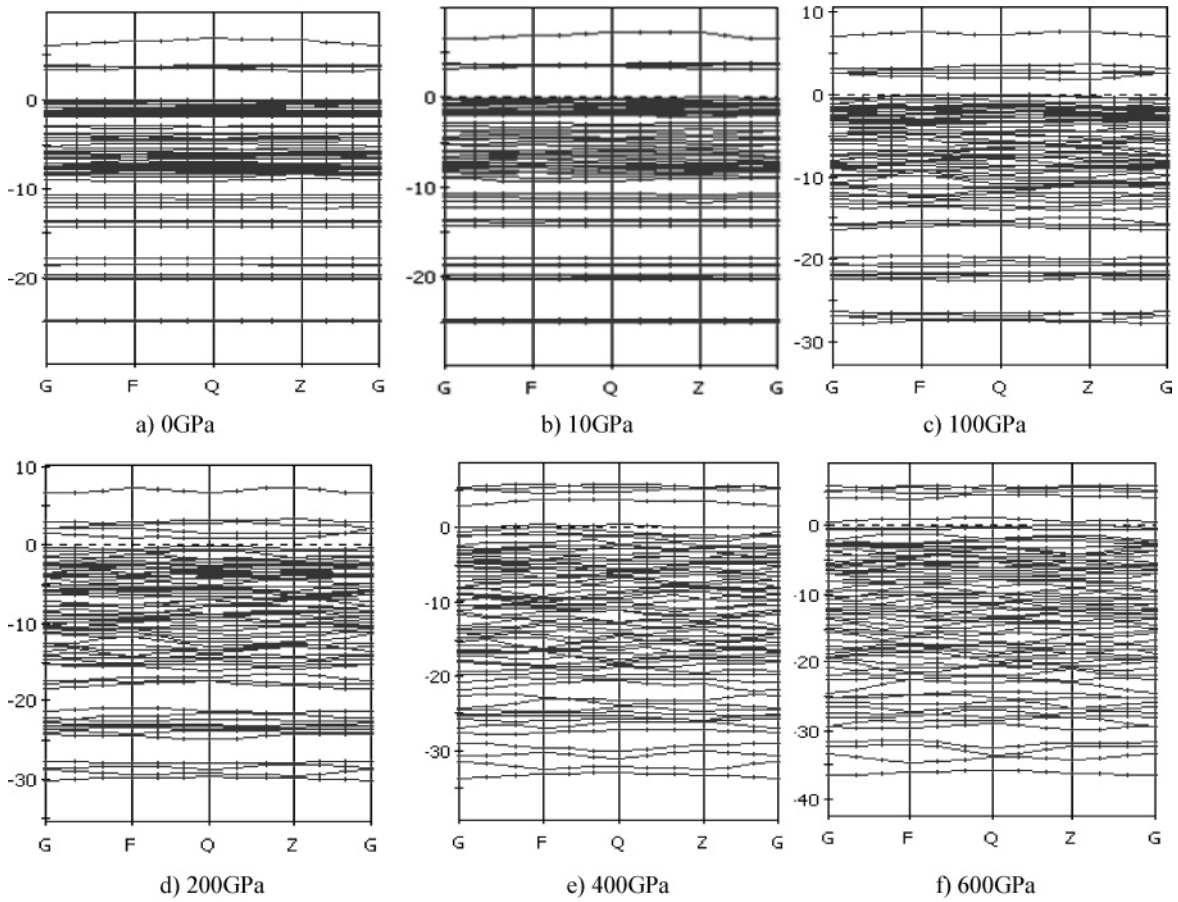

Figure 5. Calculated band structure for TNAD at different pressures.

ing to different atoms can be identified clearly in the total DOS spectrum except in the regions between (−8, −6) eV and (−2, −1) eV where there is a mixing of states, consistent with the molecular character of the crystal. A comparison of the results in Figure 4a−f shows that the upper valence band (i.e., HOCO) stems from the contributions of C(2p), N(2p), O(2p), and H(1s), with the exception of nitro-N atoms (i.e., N11, N14, N17, and N20). The bottom of the conduction band or the lowest unoccupied crystalline orbital (LUCO) between 2.6 and 4.4 eV mainly arises from the contributions of N(2p) and O(2p), and also a little from those of C(2p) and H(1s).

Additional insight into the pressure effect on the electronic structures of TNAD has been obtained from calculating the band structure and density of states in the pressure range of 0−600 GPa. Selected results of these calculations are presented in Figures 5 and 6. From the analysis of these plots, it appears that a pressure less than 10 GPa has a minor effect on the electronic structure of the crystal. The band structure (Figure 5a and b) and density of states (Figure 6a and b) both scarcely change with the increasing pressure. Both the upper valence bands and the lower conduction bands are generally flat along the Brillouin zone, and the band gap of the crystal only decreases slightly from 3.27 to 3.16 eV as the pressure increases from 0 to 10 GPa. However, as the pressure reaches over 10 GPa, increasing the pressure has several major effects on the electronic structures of the crystal. First, there is a significant increase in the bandwidth of different groups; moreover, the effect initially occurs at the upper valence bands and then extends toward the deeper bands at higher pressures (see Figure 5c−f). This broadening of the bands leads to almost a continuum of states for the higher pressure investigated here (see Figure 6e and f). Additionally, it can be seen that the bands are less and less flat across the Brillouin zone and all shift toward negative values with the increasing pressure. The band gap of the crystal decreases to about 1.0 eV at 200 GPa and to nearly zero at 600 GPa. This rapid closure of the band gap indicates that there is a change in the conduction character of the crystal from an insulator toward a metallic system. These results also support the above results related to the variations of atomic charges and bond overlap populations as well as inter- and intramolecular geometrical parameters.

3.2. Molecular Dynamics Simulations. *3.2.1 Choice of Force Field and Equilibrium of System.* The advanced Compass force field[26] was chosen to simulate the TNAD crystal, because, on one hand, the parameters of the Compass force field have been debugged and ascertained from the ab initio calculations and optimized according to experimental values, and its nonbond parameters have been further amended by the thermal physical properties of liquid and crystal molecules obtained using the MD method. On the other hand, we have employed this Compass force field to the nitramine compound HMX, and the results are in good agreement with those from experiments.[25c] Here, TNAD also belongs to the nitramine series, and it is therefore suitable to perform MD simulations on it by using the Compass force field.

The system equilibrium is ascertained by the equilibrium in temperature and energy simultaneously, that is to say, the fluctuations of temperature and energy are in the range of 5−10%. Figure 7 shows the equilibrium curves of the temperature and energy in the MD simulation of TNAD at 298 K for the latter 50 000 steps during the process of equilibration runs. It can be observed that the temperature reached the equilibrium state indeed as it fluctuates within ±10 K or so. The deviations of potential energy and nonbond energy are less than 1.4% and

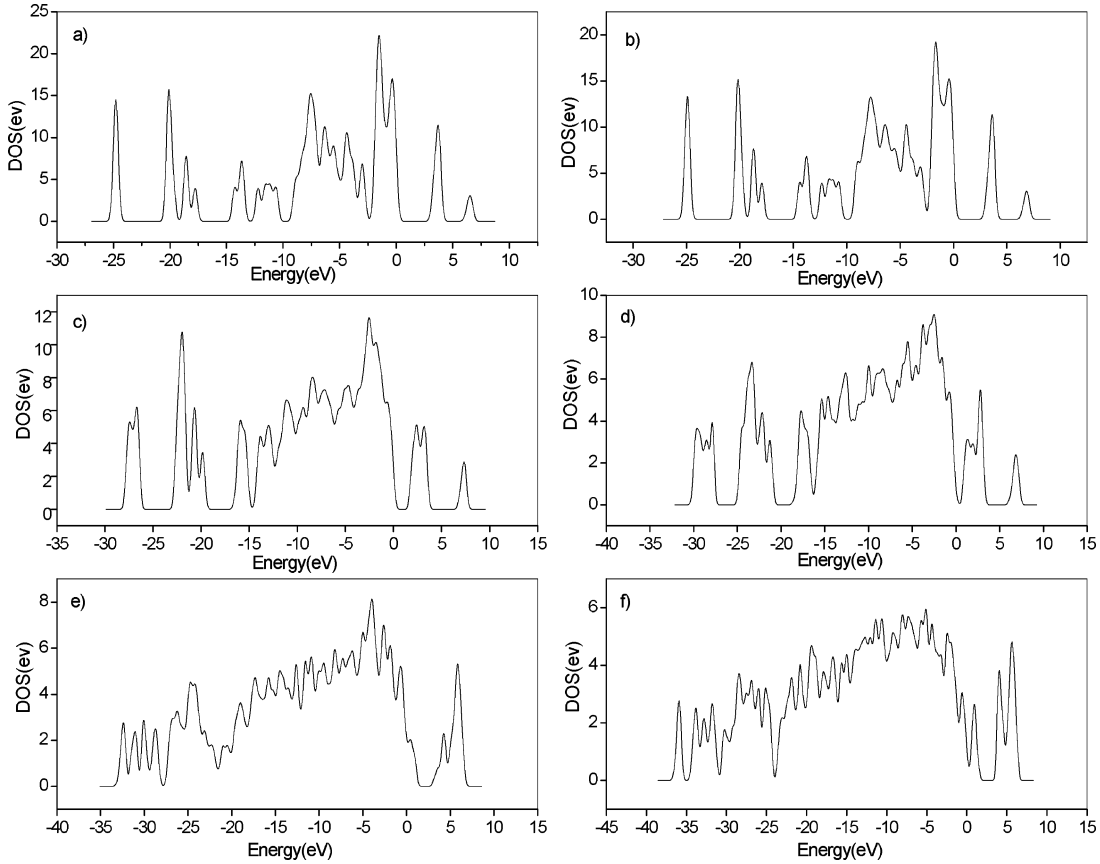

Figure 6. Calculated DOS for TNAD at different pressures: (a) 0; (b) 10; (c) 100; (d) 200; (e) 400; (f) 600 GPa.

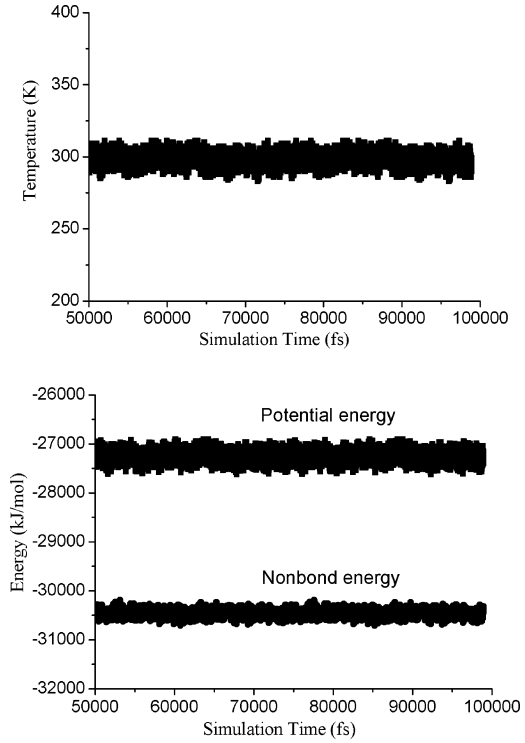

Figure 7. Temperature and energy fluctuation curves of TNAD at 298 K in the NPT-MD simulations.

0.9%, respectively, which shows that the system has reached the energy equilibrium. The system at other temperatures all comes to the equilibrium according to these two criteria. Production runs of 200 ps were performed after the equilibration runs finished. One trajectory of the coordinate for the system was collected every 1000 time steps and a total of 200 trajectory files were obtained.

3.2.2. Crystal Structure. A more realistic prediction of the lattice parameters can be obtained by considering the molecular motion as a function of temperature and pressure. For this purpose, we investigate the structural properties of TNAD during NPT runs at ambient pressure and with increasing temperature in the range of 5−500 K. The results are summarized in Table 6. It is found that the computed results are in reasonable agreement with the experimental data over the temperature range of 5−298 K, demonstrating a total volume change from −2.19% to 4.66%. In this range, the temperature does not dramatically alter the lattice dimensions. The predicted values for the lattice parameters shift slightly and agree with the experimental data in general. However, at the higher temperature range (above 350 K), the calculated results deviate largely from the experimental data; for example, at 500 K, the errors between theoretical and experimental lattice dimensions are 6.96%, 20.28%, and 2.13% for *a*, *b*, and *c*, respectively. For the entire temperature range, thermal expansion of the crystal is anisotropic with the largest expansion occurring along the *b* crystallographic axis, but with smaller changes along the *a* and *c* axes. This can also be obtained from the linear and volume expansion coefficients at 298 K (see Table 6) determined from the temperature dependence of the lattice parameters, respectively. The knowledge of thermal expansivity can help to constrain other important parameters such as the Grüneisen parameters and Rayleigh number. At present, no experimental data or previous study are available to which the calculated thermal coefficients can be compared, and it is hoped that these results will stimulate measurement of these properties. Moreover, the cell angles β and γ in the simulated TNAD unit cell remain increasing constantly as the temperature increases, while the

TABLE 6: Predicted Lattice Parameters for TNAD as Functions of Temperature from NPT-MD Simulations[a]

	lattice parameters							
T (K)	a (Å)	b (Å)	c (Å)	α (deg)	β (deg)	γ (deg)	V (Å^3)	ρ (g/cm^3)
exp (ref 7b)	6.461	6.845	7.542	74.010	75.000	68.530	293.704	1.822
5	6.399(−0.96)	6.577(−3.92)	7.430(−1.49)	73.660(−0.47)	78.639(4.85)	74.971(9.40)	287.268(−2.19)	1.862(2.20)
50	6.410(−0.79)	6.591(−3.71)	7.460(−1.09)	73.669(−0.46)	79.256(5.67)	75.135(9.64)	289.805(−1.33)	1.846(1.32)
100	6.418(−0.67)	6.602(−3.55)	7.488(−0.72)	73.679(−0.45)	80.060(6.75)	75.300(9.88)	292.903(−0.27)	1.827(0.27)
150	6.438(−0.36)	6.625(−3.21)	7.524(−0.24)	73.716(−0.40)	80.786(7.71)	75.393(10.01)	296.103(0.82)	1.807(−0.82)
200	6.452(−0.14)	6.632(−3.11)	7.551(0.12)	73.746(−0.36)	81.762(9.02)	75.550(10.24)	299.656(2.03)	1.786(−1.98)
250	6.475(0.22)	6.656(−2.76)	7.599(0.76)	73.757(−0.34)	82.962(10.62)	75.842(10.67)	303.193(3.23)	1.765(−3.13)
273	6.489(0.43)	6.665(−2.63)	7.612(0.93)	73.774(−0.32)	83.220(10.96)	75.878(10.72)	305.278(3.94)	1.753(−3.79)
298	6.499(0.59)	6.698(−2.15)	7.636(1.25)	73.813(−0.27)	84.338(12.45)	75.886(10.73)	307.397(4.66)	1.741(−4.45)
350	6.569(1.67)	6.739(−1.55)	7.662(1.59)	73.879(−0.18)	86.130(14.84)	75.963(10.85)	314.795(7.18)	1.700(−6.70)
400	6.735(4.24)	6.926(1.18)	7.680(1.83)	75.019(1.36)	91.064(21.42)	76.152(11.12)	323.740(10.23)	1.653(−9.28)
450	6.857(6.13)	7.730(12.93)	7.689(1.95)	75.278(1.71)	95.015(26.69)	76.608(11.79)	330.053(12.38)	1.621(−11.03)
500	6.911(6.96)	8.233(20.28)	7.703(2.13)	75.307(1.75)	95.899(27.87)	76.827(12.11)	331.849(12.99)	1.613(−11.47)
χ[b]	156.9× 10^{-6}	382.2× 10^{-6}	77.1× 10^{-6}				309.3× 10^{-6}	

[a] The values in parentheses correspond to the percentage differences relative to the experimental data. [b] The calculated thermal expansion coefficients of TNAD at 298 K are indicated, and the units for the linear and volume expansion coefficients are inverse kelvin.

TABLE 7: Predicted Elastic Constants (in GPa) of TNAD as Functions of Temperature

T (K)	C_{11}	C_{22}	C_{33}	C_{44}	C_{55}	C_{66}	C_{12}	C_{13}	C_{14}	C_{15}	C_{16}	C_{23}	C_{24}	C_{25}	C_{26}	C_{34}	C_{35}	C_{36}	C_{45}	C_{46}	C_{56}
5	29.4	22.1	28.3	3.5	4.1	8.3	4.6	4.4	0.2	−1.1	2.1	7.3	3.5	−1.0	−2.3	0.2	4.6	−4.8	−0.2	0.3	1.6
50	27.5	20.5	25.9	3.3	3.7	7.7	4.0	3.5	0.2	−1.0	1.9	6.6	3.2	−0.8	−2.2	0.3	4.4	−4.3	−0.1	0.3	1.5
100	26.2	19.4	24.5	3.2	3.5	7.3	3.7	2.9	0.2	−0.8	1.8	6.0	3.0	−0.6	−2.1	0.3	4.4	−4.0	−0.2	0.2	1.6
150	23.3	16.8	22.6	2.9	3.0	7.0	2.9	1.9	0.2	−0.4	1.5	5.5	2.6	−0.3	−2.1	0.5	4.2	−3.9	−0.2	0.2	1.7
200	22.1	16.4	22.1	2.7	2.7	6.9	2.7	1.6	0.2	0.1	1.4	5.3	2.7	0.0	−2.0	0.6	4.1	−3.8	−0.3	0.1	1.8
250	19.2	14.5	19.9	2.7	2.2	6.4	2.6	1.5	0.3	0.2	1.1	4.8	2.3	0.1	−1.9	0.8	3.6	−3.6	−0.2	0.0	1.6
273	18.7	14.3	19.5	2.5	2.1	6.1	2.3	1.4	0.3	0.3	1.1	4.7	2.3	0.1	−1.8	0.8	3.4	−3.2	−0.3	0.0	1.6
298	17.2	12.5	18.6	2.5	1.7	6.0	2.3	1.4	0.1	0.8	1.0	4.8	2.0	0.2	−1.7	0.9	2.5	−3.2	−0.4	−0.2	1.5
350	12.9	10.7	14.8	2.5	1.3	4.9	2.1	1.1	0.5	0.9	1.0	4.3	1.6	0.2	−1.4	0.9	1.1	−3.1	−0.5	−0.3	1.2
400	10.6	6.7	9.1	2.4	1.3	3.7	2.0	0.9	0.5	0.3	1.0	3.8	−0.2	0.3	−1.0	1.1	−0.9	−2.6	−0.5	−0.2	0.7
450	9.5	5.9	5.9	1.5	1.3	1.8	1.9	0.8	0.4	0.4	−0.6	2.5	−1.9	0.5	0.5	0.9	−0.9	0.4	−0.6	−0.3	0.8
500	9.4	5.5	5.9	1.4	1.2	1.8	1.8	0.8	0.3	0.5	−1.0	2.3	−1.9	0.6	0.9	0.9	−0.9	0.9	−0.6	−0.6	0.6

TABLE 8: Predicted Isotropic Mechanical Properties of TNAD as Functions of Temperature

T (K)	tensile modulus (GPa)	bulk modulus (GPa)	shear modulus (GPa)	Poisson's ratio	Lamé coefficient λ	Lamé coefficient μ
5	24.81	12.49	10.61	0.17	5.41	10.61
50	23.12	11.32	9.97	0.16	4.67	9.97
100	22.08	10.58	9.58	0.15	4.19	9.58
150	19.97	9.25	8.76	0.14	3.41	8.76
200	19.33	8.85	8.51	0.14	3.18	8.51
250	17.23	7.65	7.66	0.12	2.55	7.66
273	16.78	7.58	7.42	0.13	2.63	7.42
298	15.25	7.29	6.62	0.15	2.88	6.62
350	11.72	6.20	4.94	0.18	2.90	4.94
400	7.63	4.65	3.11	0.23	2.58	3.11
450	7.38	4.22	3.06	0.21	2.17	3.06
500	7.33	4.38	3.01	0.22	2.38	3.01

cell angle α changes a little compared with the experimental data in the entire temperature range of 5−500 K.

3.2.3. Mechanical Properties. On the basis of the NPT-MD simulation trajectories and the elastic-static method, the second-order elastic tensors of the TNAD crystal at atmospheric pressure in the temperature range of 5−500 K have been studied. Each structure is subjected to uniaxial tensile and pure shear deformations by the MS program, and then, the stress tensors are obtained from the Virial formalism in atomistic calculations. Consequently, the elastic coefficient matrix can be estimated from the first derivatives of the stress with respect to strain.[41] The tensile (Young's) modulus and Poisson's ratio are computed from the least-squares fits of the average tensile stress vs tensile strain and of the (negative) average lateral strain vs tensile strain, respectively. Further, other effective isotropic mechanical properties such as the shear and bulk modulus and Lamé coefficients can be calculated.

Generalized Hook's law states the most general relation of a material between stress and strain, i.e., a stress can be expressed by the linear combination of strains and the coefficient C_{ij} is an element of the elastic coefficient matrix of 6×6. In principle, all mechanical properties of a material can be derived from its elastic coefficient matrix. Because of the existence of the strain energy, the elastic coefficient matrix of a bulk should satisfy the formula $C_{ij} = C_{ji}$ even for an extremely anisotropic body, and there are 21 independent elastic constants. The symmetry can further reduce the number of independent elastic coefficients. For an isotropic solid, there are only 2 independent elastic constants. Accordingly, each modulus and Possion's ratio can be obtained from two Lamé coefficients. The program can assume a material as isotropic and calculate the effective isotropic mechanical properties.

The calculated elastic constants and effective isotropic mechanical properties (tensile modulus, bulk modulus, shear modulus, Poisson's ratio, and Lamé coefficients) of bulk TNAD were collected in Tables 7 and 8, respectively. To the best of our knowledge, there are no experimental studies or theoretical predictions on the elastic constants and the stress−strain

relationship for TNAD. So, we cannot make any comparison but only predict and compare the results at different temperatures. The results in Table 7 indicate considerable anisotropy in the diagonal elements of the tensor for TNAD ($C_{11} \approx C_{33} \approx 1.4C_{22}$; $C_{44} \approx C_{55} \approx 0.5C_{66}$). This presumably arises from the crystal packing. The larger C_{11}, C_{22}, and C_{33} imply that to reach the same strain TNAD needs a larger stress, which is consistent with its crystal structure. Furthermore, it is found that the elastic constants all decrease in general with the increasing temperature. This suggests that to reach the same strain TNAD needs a smaller stress in higher temperature ranges. An interesting observation for TNAD is that variations of the elastic constants are quite obvious and the decrement with the increasing temperature is larger in the temperature range of 5−400 K, while the variations become obscure and some elastic constants almost stay constant when the temperature is over 400 K. This suggests that there may be a glass transition for the crystalline TNAD at ca. 400 K, which is consistent with the variations of the crystallographic parameters with the changing temperature.

From the data in Table 8, it can be found that all the isotropic moduli (tensile, bulk, and shear) decrease with the increasing temperature. This indicates that the mechanical properties of TNAD have been improved effectively as the temperature increases, i.e., the rigidity and brittleness of the solid decrease while its elastic and plastic properties increase strongly. This is because the internal free volume is expanded much and the molecules within the bulk get more kinetic energy when the temperature increases. All of these changes make the material deform more easily as it is subjected to an external force, namely, the moduli decrease. It is also interesting to note that the decrease of the isotropic mechanical properties is evident in the temperature range of 5−400 K, while they change slightly and almost stay invariable when the temperature is over 400 K. Comparison of the Poisson's ratios at different temperatures shows that the Poisson's ratio decreases from 0.17 to 0.13 as the temperature increases from 5 to 250 K, while it increases with the increasing temperature from 273 K. When the temperature is over 400 K, the Poisson's ratio of bulk TNAD exceeds 0.2. This suggests that TNAD possesses some properties of a plastic at temperatures over 400 K since the Poisson's ratio of plastic is usually 0.2−0.4. This supports the above conclusion that there may be a glass transition temperature for the crystalline TNAD at about 400 K, which is drawn from the variations of the crystallographic parameters and the elastic constants.

Since PBXs with good safety and mechanical properties have been widely used in many civilian and military fields for a long time,[42−45] these results would provide valuable information for material designs of PBXs with TNAD as the main body held together by a small amount of one or more kinds of polymeric binders. This is of practical significance because the explosives used in practice are usually the mixing ones but not the compounds, such as the typical mixing PBXs, whose formulation needs theoretical guidance urgently. This also follows the chemistry development trend from "molecule chemistry" to "material chemistry".

4. Conclusions

In this study, we have performed periodic DFT calculations and classic MD simulations to investigate the geometric, electronic, and dynamic properties of the low sensitivity explosive TNAD. The effects of external stimuli such as hydrostatic pressure and temperature on TNAD have been also investigated. The major findings of this work can be summarized as follows.

(1) The calculated crystal structures and geometrical features compare well with experimental data. The calculations provide a better characterization of both the intra- and intermolecular hydrogen bonding parameters than that based on experiment.

(2) The calculations and analyses of band structure and density of states indicate that TNAD is an electrical insulator with a band gap of 3.27 eV. The top of the valence band is represented by most of the atoms in TNAD except the nitro-N atoms (N11, N14, N17, and N20). The bottom of the conduction band is mainly formed by the contributions of N(2p) and O(2p), and a little from that of C(2p) and H(1s).

(3) The compressibility of TNAD is anisotropic in the pressure range of 0−600 GPa. The structure is much stiffer in the *b* and *c* directions than along the *a* direction. Pressures less than 10 GPa have little effect on the crystal and electronic structures of TNAD; when the pressure is over 10 GPa, increasing the pressure determines significant changes of the geometrical and electronic properties of the crystal. The band gap decreases slightly from 3.27 to 3.16 eV from 0 to 10 GPa, followed by a sharp decrease to 1.0 eV at 200 GPa and to nearly zero at 600 GPa. The electronic character of the crystal changes from an insulator toward a metallic system.

(4) The linear and volume thermal expansion coefficients determined from the temperature dependence of the average lattice dimensions show that thermal expansion of the crystal is anisotropic and that the largest expansion occurs along the *b* axis. In the lower temperature range ($T < 400$ K), increasing the temperature has a little effect on the lattice parameters, which shift slightly and agree with the experimental data in general. Meanwhile, temperatures over 400 K have a strong effect on the lattice dimensions.

(5) The predicted elastic constants indicate the considerable anisotropy of bulk TNAD. Variations of the elastic constants and isotropic moduli are quite obvious, and the decrement with the increasing temperature is larger in the temperature range of 5−400 K, while the variations become obscure and some elastic properties almost stay constant when the temperature is over 400 K. The results indicate that the mechanical properties of TNAD are improved effectively as the temperature increases.

Acknowledgment. We are very grateful for the financial support from the National Natural Science Foundation of China (Grant Nos. 10576030 and 10576016) and the Innovation Project for Postgraduates in the Universities of Jiangsu Province.

References and Notes

(1) Borman, S. *Chem. Eng. News* **1994**, *72*, 18.
(2) Olah, G. A.; Squire, D. R. *Chemistry of energetic materials*; Academic Press: San Diego, 1991.
(3) Xiao, H. M. *Structures and properties of energetic compounds*; National Defence Industry Press: Beijing, 2004.
(4) Kamlet, M. J.; Jacobs, S. J. *J. Chem. Phys.* **1968**, *48*, 23.
(5) Willer, R. L. *Propellants, Explos. Pyrotech.* **1983**, *8*, 65.
(6) (a) Brill, T. B.; Oyumi, Y. *J. Phys. Chem.* **1986**, *90*, 2679. (b) Brill, T. B.; Oyumi, Y. *J. Phys. Chem.* **1986**, *90*, 6848. (c) Oyumi, Y.; Brill, T. B. *Combust. Flame* **1987**, *68*, 209.
(7) (a) Lowe-Ma, C. K. *Acta Crystallogr. C* **1990**, *46*, 1029. (b) Lowe-Ma, C. K.; Willer, R. L. Private communication, 1990.
(8) Politzer, P.; Murray, J. S.; Lane, P.; Sjoberg, P.; Adolph, H. G. *Chem. Phys. Lett.* **1991**, *181*, 78.
(9) Prabhakaran, K. V.; Bhide, N. M.; Kurian, E. M. *Thermochim. Acta* **1995**, *249*, 249.
(10) (a) Zeman, S. *Thermochim. Acta* **1997**, *302*, 11. (b) Zeman, V.; Koci, J.; Zeman, S. *Energetic Materials* **1999**, *7*, 172. (c) Zeman, S.; Koci, J. *Energ. Mater.* **2000**, *8*, 18.
(11) Sorescu, D. C.; Rice, B. M.; Thompson, D. L. *J. Phys. Chem. A* **1998**, *102*, 8386.
(12) Liu, M. H.; Chen, C.; Hong, Y. S. *J. Mol. Struct. (THEOCHEM)* **2004**, *710*, 207.

(13) Qiu, L.; Xiao, H. M.; Ju, X. H.; Gong, X. D. *Int. J. Quantum Chem.* **2005**, *105*, 48.
(14) Bardo, R. D. *Shock waves in condensed matter*; Gupta, Y. M., Ed.; Plenum Press: New York, 1985.
(15) Coffey, S. F. *Phys. Rev. B* **1981**, *24*, 6984.
(16) Gilman, J. J. *Philos. Mag. B* **1993**, *78*, 207.
(17) Sorescu, D. C.; Rice, B. M.; Thompson, D. L. *J. Phys. Chem. B* **1999**, *103*, 6783.
(18) Sorescu, D. C.; Thompson, D. L. *J. Phys. Chem. A* **2001**, *105*, 720.
(19) Sorescu, D. C.; Thompson, D. L. *J. Phys. Chem. A* **2001**, *105*, 7413.
(20) Wu, C. J.; Yang, L. H.; Fried, L. E. *Phys. Rev. B* **2003**, *67*, 235101.
(21) Yang, X. Z. *Molecular Simulation and Macromolecule Material*; Science Press: Beijing, 2002.
(22) Thomas, D. S.; Ralph, M.; Dmitry, B.; Grant, D. S. *J. Chem. Phys.* **2003**, *119*, 7417.
(23) Gee, R. H.; Roszak, S.; Balasubramanian, K.; Fried, L. E. *J. Chem. Phys.* **2004**, *120*, 7059.
(24) (a) Sorescu, D. C.; Boatz, J. A.; Thompson, D. L. *J. Phys. Chem. A* **2001**, *105*, 5010. (b) Sorescu, D. C.; Thompson, D. L. *J. Phys. Chem. B* **1999**, *103*, 6774. (c) Velardez, G. F.; Alavi, S.; Thompsona, D. L. *J. Chem. Phys.* **2003**, *119*, 6698.
(25) (a) Li, J. S.; Xiao, H. M.; Dong, H. S. *Explos. Impulsion* **2000**, *20*, 221. (b) Xiao, H. M.; Li, J. S.; Dong, H. S. *J. Phys. Org. Chem*. **2001**, *14*, 644. (c) Xiao, J. J.; Fang, G. Y.; Ji, G. F.; Xiao, H. M. *Chin. Sci. Bull.* **2005**, *50*, 21. (d) Xiao, J. J.; Huang, Y. C.; Hu, Y. J.; Xiao, H. M. *Sci. China B* **2005**, *48*, 21. (e) Huang, Y. C.; Hu, Y. J.; Xiao, J. J. *Chin. J. Phys. Chem*. **2005**, *21*, 425. (f) Ma, X. F.; Xiao, J. J.; Yin, K. L.; Xiao, H. M. *Chin. J. Chem. Phys.* **2005**, *18*, 55. (g) Xiao, J. J.; Gu, C. G.; Fang, G. Y.; Xiao, H. M. *Acta Chim. Sin.* **2005**, *63*, 439. (h) Xiao, J. J.; Hu, Y. J.; Huang, Y. C.; Xiao, H. M. *Sci. China B* **2005**, *47*, 504.
(26) Sun, H. *J. Phys. Chem. B* **1998**, *102*, 7338.
(27) Payne, M. C.; Teter, M. P.; Allan, D. C.; Arias, T. A.; Joannopoulos, J. D. *Rev. Modern Phys.* **1992**, *64*, 1045.
(28) Vanderbilt, D. *Phys. Rev. B* **1990**, *41*, 7892.
(29) Kresse, G.; Furthmüller, J. *Phys. Rev. B* **1996**, *54*, 11169.
(30) Fischer, T. H.; Almlof, J. *J. Phys. Chem.* **1992**, *96*, 9768.
(31) Ceperley, D. M.; Alder, B. J. *Phys. Rev. Lett.* **1980**, *45*, 566.
(32) Perdew, J. P.; Zunger, A. *Phys. Rev. B* **1981**, *23*, 5048.
(33) Monkhorst, H. J.; Pack, J. D. *Phys. Rev. B* **1976**, *13*, 5188.
(34) *Materials Studio 3.0*; Accelrys Inc.: San Diego, CA, 2004.
(35) Andersen, H. C. *J. Chem. Phys.* **1980**, *72*, 2384.
(36) Parrinello, M.; Rahman, A. *J. Chem. Phys.* **1982**, *76*, 2662.
(37) Allen, M. P.; Tindesley, D. J. *Computer Simulation of Liquids*; Oxford University Press: New York, 1989.
(38) Fiorentini, V. *Phys. Rev. B* **1992**, *46*, 2086.
(39) Mulliken, R. S. *J. Chem. Phys.* **1955**, *23*, 1833.
(40) (a) Harris, N. J.; Lammertsma, K. *J. Phys. Chem. A* **1997**, *101*, 1370. (b) Oxley, J. C.; Kooh, A. B.; Szekeres, R.; Zheng, W. *J. Phys. Chem.* **1994**, *98*, 7004. (c) Oxley, J. C.; Hiskey, M.; Naud, D.; Szekeres, R. *J. Phys. Chem.* **1992**, *96*, 2505. (d) Capellos, C.; Papagiannakopoulos, P.; Liang, Y. L. *Chem. Phys. Lett.* **1989**, *164*, 533. (e) Zuckermann, H.; Greenblatt, G. D.; Haas, Y. *J. Phys. Chem.* **1987**, *91*, 5159.
(41) Weiner, J. H. *Statistical Mechanics of Elasticity*; John Wiley: New York, 1983.
(42) Sun, G. X. *Polymer Blended Explosives*; Defense Industry Press: Beijing, 1984.
(43) Dobratz, B. M.; Crawford, P. C. *LLNL explosives handbook-properties of chemical explosives and explosive simulants*; UCRL-52997, Lawrence Livermore National Laboratory: Livermore, CA, 1985.
(44) Hoffman, D. M.; Caly, L. E. *Polym. Eng. Sci*. **1986**, *26*, 1489.
(45) Sun, Y. B.; Hui, J. M.; Cao, X. M. *Military Use Blended Explosives*; Weapon Industry Press: Beijing, 1995.